Author Manuscript

Author Manuscript

Author Manuscript

Author Manuscript

HHS Public Access

Author manuscript

Biochemistry. Author manuscript; available in PMC 2017 March 01.

Published in final edited form as:

Biochemistry. 2016 March 01; 55(8): 1254–1264. doi:10.1021/acs.biochem.5b00732.

Molecular modeling of the structural and dynamical changes in calcium channel TRPV5 induced by the African-specific A563T variation

Lingyun Wang[1], **Ross P. Holmes**[2], and **Ji-Bin Peng**[1,2,*]

[1]Division of Nephrology, Department of Medicine, Nephrology Research and Training Center, University of Alabama at Birmingham, Birmingham, AL 35294

[2]Department of Urology, University of Alabama at Birmingham, Birmingham, AL 35294

Abstract

TRPV5 (Transient Receptor Potential cation channels, Vanilloid subfamily, member 5) plays a key role in active Ca^{2+} reabsorption in the kidney. Variations in TRPV5 occur at high frequency in African populations and may contribute to their higher efficiency in Ca^{2+} reabsorption. One of the African specific variations, A563T, exhibits increased Ca^{2+} transport ability. However, it is unclear how this variation influences the channel pore. Based on the structure of TRPV1, a TRPV5 model was generated to simulate the structural and dynamical changes induced by the A563T variation. Based on this model, amino-acid residue 563 interacts with V540, which is one residue away from the key residue D542 involved in Ca^{2+} selectivity and Mg^{2+} blockade. The A563T variation increases secondary structure stability and reduces dynamical motion of D542. In addition, the A563T variation alters electrostatic potential of the outer surface of the pore. Differences in contact between selective filter residues and residue 563 and in electrostatic potential between the two TRPV5 variants were also observed in another model derived from an alternative alignment in the selective filters between TRPV5 and TRPV1. These findings indicate that the A563T variation induces structural, dynamical, and electrostatic changes in the TRPV5 pore, providing a structural insight into the functional alterations associated with the A563T variation.

Graphical abstract

*To whom correspondence should be addressed: Division of Nephrology, Department of Medicine, University of Alabama at Birmingham, ZRB 625, 1900 University Boulevard, Birmingham, AL 35294-0006, jpeng@uab.edu.

SUPPORTING INFORMATION

This provides a detailed description of the correlation between monomers, detailed simulation results for the alternative model, sequence alignment of TRPV5 with TRPV1 (Figure S1), TRPV5 pore (residues 473-595) in a POPC (1-palmitoyl-2-oleoyl-sn-glycero-3-phosphocholine) membrane-like environment (Figure S2), equilibration of the two TRPV5 systems (Figure S4), change of helix occupancy for the regions around residue 563 (Figure S5), dynamical change of Ca^{2+} ions (Figure S6), structural (Figure S7, S8, and S13), dynamical (Figures S10 and S12) and electrostatic (Figure S11) analyses for the alternative model, evaluation of TRPV5 models created by MODELLER (Table S1) and the averaged RMSD (root mean square deviation) values for each monomer of TRPV5 during the last 200 ns simulation (Table S2). This supporting material is available free of charge via the Internet at http://pubs.acs.org.

Author Manuscript Author Manuscript Author Manuscript Author Manuscript

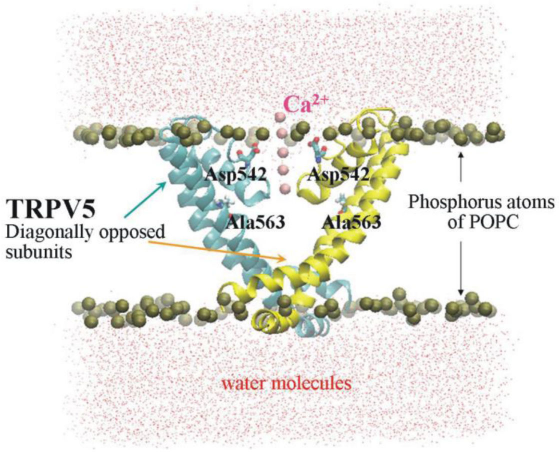

Keywords

TRPV5; single nucleotide polymorphisms (SNPs); Ca^{2+} reabsorption; molecular dynamics simulation

1. INTRODUCTION

Calcium (Ca^{2+}) plays an important role in physiological processes such as muscle contraction, bone formation, and intracellular signaling (1-3). Ca^{2+} balance is maintained by intestinal absorption, renal reabsorption, as well as Ca^{2+} deposition in and mobilization from bone (4, 5). Each of these processes is physiologically important. For instance, a disturbance in renal Ca^{2+} reabsorption may lead to disorders such as kidney stone disease, osteoporosis, and vitamin D-resistant rickets (6-9).

Ca^{2+} absorption and reabsorption involve a transcellular pathway for Ca^{2+} ions to enter the body across epithelia. In this pathway, Ca^{2+} in the intestinal lumen or glomerular filtrate first crosses the apical plasma membrane and enters epithelial cells down a steep Ca^{2+} gradient. Two epithelial Ca^{2+} channels, TRPV5 and TRPV6, are responsible for this process (9, 10). Once Ca^{2+} ions get into the cell, they bind to Ca^{2+} binding proteins so that intracellular free Ca^{2+} concentration will not reach a level toxic to the cells. Ca^{2+} ions exit the cell by crossing the basolateral membrane via Na^{+}/Ca^{2+} exchangers and/or Ca^{2+} pumps. Compared to the paracellular pathway where Ca^{2+} ions passively enter the body through tight junctions between epithelial cells, the transcellular pathway allows Ca^{2+} ions to be transported against a chemical gradient. This pathway is the major target of 1,25-dihydroxylvitamin D_3 and is rigorously regulated under physiological conditions such as pregnancy and lactation (11). Because epithelial Ca^{2+} channels mediate the first step in the transcellular pathway for Ca^{2+} transport, they are considered as gatekeepers for Ca^{2+} absorption and reabsorption.

TRPV5 and TRPV6 genes are localized in a region of chromosome 7 that exhibits strong evidence of recent positive geographical selection (12, 13). In this region of chromosome 7 (7q34–35), a genetic sweep likely occurred after early humans migrated outside Africa. As a result, several non-synonymous single nucleotide polymorphisms (SNPs) in both TRPV5

Author Manuscript Author Manuscript Author Manuscript Author Manuscript

and TRPV6 genes are present at high allele frequencies in African Americans but not in European Americans. We found among the three non-synonymous SNPs in TRPV5 (A8V, A563T and L712F), A563T was most effective in increasing TRPV5-mediated Ca^{2+} uptake by altering the function of the channel (14). This is consistent with the fact that A563T is distributed to the last transmembrane (TM) domain of TRPV5 and could affect Ca^{2+} transport by a mechanism not well understood. This A563T variation occurs at an allele frequency of approximately 10% in African Americans. Thus, it may have substantial impact on Ca^{2+} reabsorption among African Americans and other populations of African origin.

TRPV5 belongs to the 6-membered Transient Receptor Potential Vanilloid family, which are highly conserved in gene exon-intron arrangements and protein structure (15, 16). The common structural feature of these channels include an intracellularly localized amino-terminus consisting of 6 Ankyrin repeats, followed by six TM domains (designated TM1-TM6) with a pore region formed between TM5 and TM6, and an intracellular carboxyl terminus. The functional unit of the channels in this family is a tetramer. Although residue 563 is 21 residues away from the aspartate residue at 542, which forms a Ca^{2+} filter in the channel (17, 18), these two residues may interact in a 3-dimentional and dynamical model. Recently, the structure of the first member of the family, TRPV1, has been solved by high-resolution electron cryo-microscopy (19, 20). This provides an opportunity to examine how the A563T variation alters the channel function from a structural point of view.

In this study, we constructed the TRPV5 model based on the structure of TRPV1, which is over 30% identical to TRPV5 in primary sequence and is identical to TRPV5 in gene structure organization. Using this model, the structural, dynamical and electrostatic alterations in the pore of TRPV5 induced by the A563T variation were simulated and new insights into the molecular basis for the functional impact of this variation were obtained.

2. MATERIALS AND METHODS

2.1 System modeling

To date, there is still no crystal structure available for TRPV5, thus homology modeling based on the structure of TRPV1 was performed to provide structural information for TRPV5. The structure of TRPV5 was modeled by using MODELLER 9.13 software (21). Using this software we generated refined three-dimensional models of the target protein TRPV5 based on its alignment with TRPV1. The template of TRPV1 was obtained from the Protein Data Bank (PDB) with the PDB ID of 3J5P. The TRPV5 structure was modeled based on the sequence alignment between TRPV1 and TRPV5 as laid out by Liao *et al.* (19). Since the pore structure of TRPV5 is formed between the fifth and sixth transmembrane helices, other parts of TRPV5 from the PDB structure were not used for modeling in order to reduce the system size due to limited simulation resources. The sequence of TRPV5 used in the modeling and simulation is shown in Figure S1a (Supporting Information). In the electron cryo-microscopic structure of TRPV1, residues 604-626 (loop between TM5 and TM6, shaded in Figure S1) were not included because these residues were deleted in the TRPV1 construct in order to obtain a biochemically stable and yet functional TRPV1 for structural studies (19). Thus, the loop was not used in the homology modeling. Sequence

Author Manuscript Author Manuscript Author Manuscript Author Manuscript

alignment between TRPV5 (model) and TRPV1 (template) was performed using ClustalW2 (22). The sequence identity was 29.31% in the corresponding region of TRPV5 and TRPV1. This is very close to the 30% amino-acid identity that is considered reliable to model membrane proteins (23).

The TRPV5 pore structure has been modeled based on its similarity to the K^+ channel KcsA when the TRPV1 structure was not available (24, 25). Taking this into consideration, an alternative alignment between TRPV1 and TRPV5 was generated (Figure S1b). The sequence identity between TRPV5 and TRPV1 increased slightly to 32.48% in this alignment; however, gaps were introduced in the pore helix and in TM6. The penalty score caused by the two gaps in the α-helix regions resulted in this alignment not being chosen by the program at the default settings.

For comparison, two modeled TRPV5 pore structures were generated based on the two sequence alignments (Figures S2a and S2b). We then compared the position of residues in the selective filter with relevant ion channels, including TRPV1 (Figure S2c; PDB ID: 3J5P), KcsA (Figure S2d; PDB ID: 1J95), and a voltage-gated Ca^{2+} channel Ca_vAb (Figure S2e; PDB ID: 4MS2). The difference between the filter residues in the two modeled structure is that D542, the key residue for Ca^{2+} permeation, is in the entrance of TRPV5 in the model shown in Figure S2a, but it locates further into the channel pore in the model shown in Figure S2b. Unlike the K^+ channel KcsA, a negatively charged aspartate residue (D646 in TRPV1 and D178 in Ca_vAb) is present in the entrance of the pore in the two Ca^{2+} permeable channels (TRPV1 and Ca_vAb). There are two aspartate residues in the pore of Ca_vAb, and Tang et al. (26) indicated that the carboxyl side chain of D178 in the pore entrance forms the first hydrated Ca^{2+}-binding site in the selectivity filter, and the substitution of D178 to S178 resulted in a 100-fold reduction in the Ca^{2+} to Na^+ permeability ratio. Nilius *et al.* (17) demonstrated that D542 in TRPV5 is critical for Ca^{2+} selectivity, and the D542A mutation markedly decreases Ca^{2+} permeability. Thus, the model in Figure S2a is compatible with that of Ca_vAb, as D542 in TRPV5 plays a role similar to that of D178 in Ca_vAb. We chose the alignment in Figure S1a to model TRPV5 structure; however, results based on the alternative alignment as presented in the supporting information were also discussed.

A set of 100 structures was generated by MODELLER. The first 10 structures with the lowest DOPE energy (PDB files provided in Supporting Information) were assessed by different statistical methods (Table S1), including ERRAT (27), PEOCHECK (28), and WHAT_CHECK (29) and VERIFY3D (30). The structure with the lowest DOPE energy, highest ERRAT value, and fewest errors checked by PROCHECK and WATCHECK was chosen as the best model. Using VMD software (31), five Ca^{2+} ions were docked into the pore of TRPV5 by superposition of the modeled structure with the structure of a voltage-gated calcium channel (PDB ID: 4MS2) (26). The A563T variation was introduced into all the four subunits of TRPV5 using the mutagenesis function of PyMOL (32). The two TRPV5 systems are denoted as TRPV5-A563 (shown as an example in Figure 1) and TRPV5-T563, respectively.

Author Manuscript Author Manuscript Author Manuscript Author Manuscript

To mimic the membrane environment, the modeled TRPV5 structures were embedded in a lipid bilayer composed of 158 POPC (1-palmitoyl-2-oleoyl-sn-glycero-3-phosphocholine) lipids by using CHARMM-GUI membrane builder (33). Each of the TRPV5 systems (TRPV5-A563 or TRPV5-T563) was then hydrated with a total of 2089 TIP3P (transferable intermolecular potential 3P) water molecules on both sides of the bilayer. The approximate dimensions of the resultant simulation box were 87 Å × 87 Å × 95 Å along the x, y and z direction, respectively, with the normal to the membrane surface along the z-direction, and its center of mass situated at the origin of the coordinate system. Na^+ and Cl^- ions were added to the system to neutralize it and maintain a 150 mM NaCl concentration (Figure S3). The parameters of a FF14SB force field (34) were assigned to the protein, ions and water molecules, and a FFlipid14 force field (35) was used for POPC lipids.

2.2 Molecular dynamics simulations

To compare the effect of the A563T variation on the structural and dynamical changes in TRPV5, we performed two 400 ns molecular dynamic (MD) simulations using the AMBER14 simulation package (36). Before production simulations, the two systems were further refined. Each system was relaxed by 5,000 steps of steepest descent followed by 5,000 steps of conjugate gradient minimization. After energy minimization of the whole system, the water molecules were equilibrated for 200 ps, while the protein, lipids and ions (including the five Ca^{2+} ions) were restrained at a constant number-pressure-temperature (NpT) at 50 K and 1 atm by applying a force constant of 100 kcal•mol^{-1}•$Å^{-1}$. Then the system was gradually heated to 300 K via six 100 ps constant number-volume-temperature (NVT) MD simulations, still maintaining the restraint on the protein, lipids and ions (including the five Ca^{2+} ions). The restraints were kept only for the five Ca^{2+} ions in the subsequent 10 ns equilibration simulation at NpT of 300 K and 1 atm by applying a force constant of 10 kcal•mol^{-1}•$Å^{-1}$. Lastly, 400 ns production simulations were carried out using Berendsen temperature and pressure coupling (37) without any restraint. The SHAKE constraints (38) were applied to all hydrogen heavy bonds to permit a dynamics time step of 2 fs. Electrostatic interactions were calculated by the particle-mesh Ewald method (PME) (39, 40) with grid spacing of 0.12 nm and interpolation of order four. Both of the direct space PME and Lennard-Jones cutoffs were set at 10 Å. The data for the MD simulations were collected every 2 ps. The simulations were performed on the AMD Opterons cluster in the Alabama Supercomputer Center.

2.3 Equilibration of the simulated systems

TRPV5-A563 and TRPV5-T563, embedded in a POPC lipid bilayer (Figure S3), underwent 400 ns MD simulations. The time-dependent root mean square deviations (RMSD) for the Ca atoms of TRPV5-A563 and TRPV5-T563 were calculated to provide an overall measure of the departure of the structures from the initial coordinates (Figure S4). It was clear that both TRPV5-A563 and TRPV5-T563 reached equilibration state after 200 ns. To further evaluate the equilibration of TRPV5, the average RMSD for each monomer of TRPV5 was calculated over the last 200 ns simulation (Table S2). The small standard deviations of the RMSD values indicated that they reached equilibration states in the last 200 ns. Thus, the last 200 ns MD simulations were used for the analyses of the effect of A563T variation on the structural and dynamical changes in TRPV5.

Author Manuscript Author Manuscript Author Manuscript Author Manuscript

2.4 Structural and dynamical Analyses

With the equilibrated MD simulation trajectories, we performed a secondary structural analysis, conformational analysis, and dynamical motion analysis to better understand the conformational, structural, and motion characteristics of TRPV5. RMSD of protein backbone atoms were analyzed to determine the system's equilibration tendencies and its convergence. We calculated the changes of the residues of α-helix occupancy for TRPV5, especially for the residues around residue 563, to evaluate secondary structural changes of the protein caused by the A563T variation. The DSSP method was used to determine whether an amino acid residue belonged to an α-helix (41). The occupancy of each residue in an α-helix was determined on the basis of the percentage of time that the residue existed in the α-helix over the simulation. The helix percentage for TRPV5 was calculated from the overall helicity divided by the total residue number. Clustering analysis was performed to get the representative structure of TRPV5 using the MMTSB toolset (42). The K-means algorithm (43) based on the RMSD similarity of the structures was used in the clustering analysis. A centroid structure was generated by averaging the PDB structures of TRPV5. The structure that had the lowest RMSD from the centroid structure was obtained as the representative structure. To study the conformational fluctuation for each residue, root-mean-square fluctuations (RMSF) of TRPV5 were calculated on a residue-by-residue basis and averaged over the equilibrated simulations. Dynamical cross-correlation maps (DCCM) between residues were calculated to provide information for correlated motion of the pair residues and the degree of the correlation (44). MATLAB (45) was used to generate the cross-correlation plots.

Principal component analysis (PCA) was performed to characterize the collective motion of TRPV5 residues. In MD simulation, both local dynamical fluctuations and collective motions of residues occur simultaneously. PCA is a multivariate statistical method to separate the collective motions from the local dynamics by reducing high-dimensional motional data sets into a small subset composed of principal components that describes the collective motion (46). PCA describes protein motions by diagonalization of the covariance matrix C_{ij} (3N*3N array) of the atomic positional deviations

$$C_{ij}=<(\mathrm{x}_i-<\mathrm{x}_i>)(\mathrm{x}_j-<\mathrm{x}_j>)>$$

where x_i, x_j is a Cartesian coordinate of a residue, and the angle brackets represent the time averages over all simulation trajectories. After the matrix diagonalized, a set of eigenvectors and eigenvalues can be obtained. The eigenvectors indicate the directions of collective motion, and the corresponding eigenvalues indicate the amplitude of the motion. The major collective motion can be represented by large eigenvalues along the eigenvectors. In this study, only the first principal component that dominates the collective motion of TRPV5 was shown.

We also analyzed the contact numbers between residue 563 and the filter residues. A contact was identified if the carbon atoms were within 5.4 Å and hydrogen atoms within 4.6 Å consistent with the work of Cheng et al. (47). All these analyses were performed using the equilibrated simulation trajectories by the ptraj program of AMBER. The electrostatic

Author Manuscript Author Manuscript Author Manuscript Author Manuscript

potential for TRPV5 was calculated by APBS (48). To calculate the electrostatic potential, dielectric constants of 1 and 78.54 were used separately for the protein and solvent, respectively. An ion concentration of 150 mM was used in the APBS calculation. The electrostatic potential was mapped onto the molecular surface of TRPV5 using VMD (31).

2.5 Statistical methods

To compare the key residue distances between TRPV5-A563 and TRPV5-T563, the average values and the standard deviations of the analyzed variables were calculated. Because the adjacent snapshots from the MD trajectory have the tendency to be correlated with each other, the autocorrelation time (49, 50) for the studied variables were obtained to re-sample the trajectories into statistically independent periods in order to calculate the standard deviations for the studied variables. With the obtained decorrelation times, bootstrap analysis was performed following steps similar to Chen and Pappu (51) and our previous study (52). Significant differences in the mean and standard deviations for the studied variables were determined using the Student's t-test (53) with 95% confidence.

3. RESULTS AND DISCUSSION

3.1 Amino-acid residue at 563 influences residues lining the ionic filter of TRPV5

In this work, a structure containing the TRPV5 pore (residues 473-595, Figure S1) was modeled based on the structure of TRPV1. In the TRPV5 model (Figure 1), residues ^{539}TVID^{542} form the selective filter of TRPV5, corresponding to ^{643}GMGD^{646} in the TRPV1 structure (Figure S1) (19). The four D542 residues in the selectivity filter form a ring in the mouth of the pore. Along the pore, another three residues, including T539, V540 and I575, form the ion pathway. We focused on the relationship between A/T563 and D542 because it is well known that D542 is involved in Ca^{2+} transport and the Mg^{2+} blockade (17, 54), which are affected in the A563T variant of TRPV5 (14). In the TRPV5 model, residue 563 is beneath D542 but not within the distance for direct interaction. This structure implies that residue 563 may mediate the Ca^{2+} transport activity indirectly.

Although A/T563 appeared not to be in direct contact with D542, it may affect D542 via other residues close to D542. We wondered to what extent residue 563 interacts with each of the filter residues ^{539}TVID^{542}. To this end, the time-dependent contact number between each filter residue and residue 563 was calculated (Figure 2a). Among these residues, V540 exhibited large contact numbers with residue 563, whereas T539, I541 and D542 showed fewer or no interactions with residue 563. Thus, V540 plays an important role in interacting with residue 563.

The interaction between V540 and residue 563 was not obvious in the initial model (Figure 1). To provide a clear structural view of how the interaction may take place, the representative structures exhibiting the interaction of V540 with residue 563 in TRPV5-A563 and TRPV5-T563 are presented in Figures 2b and 2c, respectively. The representative structures for TRPV5-A563 and TRPV5-T563 were obtained by clustering analysis. In both TRPV5-A563 and TRPV5-T563, the side chain carbon atom of V540 contacted with that of

Author Manuscript Author Manuscript Author Manuscript Author Manuscript

residue 563 in the neighboring subunit. In this way, the structural and dynamical change of residue 563 may affect D542 through the interaction between residues A/T563 and V540.

3.2 A563T variation leads to structural change in the pore of TRPV5

To assess the potential effect of A563T variation on the structural change in TRPV5, helix occupancy analyses surrounding the pore region (residues 473-595) were performed for TRPV5-A563 and TRPV5-T563 (Figure 3). The overall helix occupancy of the TRPV5 pore didn't differ substantially between TRPV5-A563 and TRPV5-T563 (66.05% vs. 67.08%). However, the helix occupancy in the region around residue 563 (residues 559 to 567, regions shaded in Figure 3) increased substantially (from 82.15% for TRPV5-A563 to 97.40% for TRPV5-T563). Thus, the A563T variation indeed results in a structural change in its vicinity. The lower helix occupancies around residue 563 were observed in monomers 3 and 4 but not in monomers 1 and 2 in TRPV5-A563. In contrast, the helix occupancies were similar among monomers of TRPV5-T563.

To further investigate the change of helix propensity for the regions around residue 563, the helix occupancy was calculated during the course of simulation (Figure S5a). The helix occupancy in the region around residue 563 decreased in both TRPV5-A563 and TRPV5-T563 along the course of the simulation. While the occupancy value of the regions in TRPV5-A563 gradually decreased to 80%, that in TRPV5-T563 maintained around 95% during the last 200 ns of simulation. Representative structures of monomer 3 in the regions around residue 563 clearly showed the helix structure was lost in TRPV5-A563 (Figure S5b), whereas it was maintained in TRPV5-T563 (Figure S5c).

The diameter of the opening of the pore is a determinant of ion transport activity. Since D542 is the critical residue for Ca^{2+}-selectivity (17, 54), the distance of the carboxylate oxygen atoms in D542 between the diagonally opposed TRPV5 monomers was chosen to represent the diameter of the TRPV5 pore. To give a clear view of the structural change caused by the A563T variation, snapshots of the representative structures representing the distance changes of the key residues are shown in Figure 4. In the initial modeled structure, the distance value of the diagonally opposed carboxylate oxygen atoms of D542 was 10.22 Å (Figure 1). Over simulation time, this distance decreases to 5.49 ± 0.61 Å in TRPV5-A563, whereas it decreases to 4.42 ± 0.21 Å in TRPV5-T563. This difference is statistically significant, indicating the A563T variation may alter the diameter of the pore. This may affect Ca^{2+} movements and Mg^{2+} blockade, which are mainly determined by D542.

Besides D542 (the selectivity residue), V540 and T539 lie along the ion transport pathway of the pore in the initial model (Figure 1). Residues V540 and T539 respectively correspond to M644 and G643 of TRPV1, which form a restriction point in the TRPV1 pore (5.9 Å for diagonally opposed M644 and 4.6 Å for diagonally opposed G643) (20). To investigate whether V540 and T539 form a restriction point for TRPV5, the distances between the diagonally opposed V540 and T539 were also calculated (Figure 4). During the equilibrated simulation, the distance between the diagonally opposed backbone carbon atoms of V540 increased to 13.89 ± 0.47 Å and 14.06 ± 0.33 Å in TRPV5-A563 and TRPV5-T563, respectively; that of T539 increased to 10.53 ± 0.45 Å and 9.84 ± 0.27 Å in TRPV5-A563 and TRPV5-T563, respectively. These results indicate that V540 and T539 are not restriction

Author Manuscript Author Manuscript Author Manuscript Author Manuscript

points in TRPV5 and they may not affect Ca^{2+} moving along the ion transport pathway in TRPV5.

The activation of TRPV1 not only involves a conformational change in the selectivity filter, but also the opening of the lower gate (residue I679) (20). In the unliganded structure of TRPV1, the distance between diagonally opposed I679 is 5.3 Å, whereas the distance increases to 9.3 Å when TRPV1 binds with its agonist. To study whether the lower gate still plays a role in TRPV5, the distance between the diagonally opposed side chain carbon atoms of I575 (corresponding to I679 in TRPV1) was also calculated (Figure 4). The averaged distance is 6.43 ± 0.37 Å in TRPV5-A563, whereas it is 6.49 ± 0.29 Å in TRPV5-T563. For both TRPV5 structures, the distance is 1.1 Å larger than the corresponding distance in unliganded TRPV1, which is still smaller than the distance in the activated TRPV1. Thus, the lower gate appears less important in Ca^{2+} influx than the selectivity filter in TRPV5. Even if it plays a critical role in Ca^{2+} transport, the A563T variation in TRPV5 does not result in significant changes in the lower gate.

3.3 A563T variation results in dynamical change in the pore of TRPV5

We next assessed the dynamical changes associated with the A563T variation in the pore region of TRPV5. The fluctuation motions of key residues, the coordinated movement of residues, and the collective motion of key residues were compared between TRPV5-A563 and TRPV5-T563.

The fluctuation motions of the region containing residues 473-595 in TRPV5 were assessed by root mean square fluctuation (RMSF). This method provides residue fluctuation motions with respect to the average position. Overall, the fluctuation of TRPV5-A563 was higher than TRPV5-T563 across the region analyzed (Figure 5a). When zoomed in, the RMSF value of D542 in TRPV5-T563 was lower than that in TRPV5-A563 (Figure 5b, left panel). The RMSF values for residues 563 and 540 were also lower in TRPV5-T563 (Figure 5b). Collectively, the sum of RMSF values for the 3 residues was significantly higher in TRPV5-A563 than in TRPV5-T563 (Figure 5c). Since residue 563 interacts with V540 in the filter, it is likely the decreased motion of T563 leads to less movement of V540, and in turn, less movement of the neighboring D542. This provides an explanation for how the A to T substitution at 563 alters the dynamics at D542, a key filter residue involved in Ca^{2+} permeability and Mg^{2+} blockade (17). Indeed, we previously observed an alteration in both Ca^{2+} uptake activity and Mg^{2+}-sensitivity in the TRPV5-T563 variant (14).

We next assessed the coordinated movement in A563 and T563 variants using a dynamics cross-correlation map (DCCM) (Figure 6). Compared to TRPV5-A563, TRPV5-T563 has less correlated motions (regions I and II in the white boxes of Figure 6) and anticorrelated motions (regions III, IV, V, VI and VII in black boxes of Figure 6) between residues in different monomers. (The correlation details between the regions of the monomers are described in the Supporting Information.) These correlation data suggest that the A563T variation result in less correlated motion among residues of TRPV5. The correlation difference took place among the TRPV5 monomers, which are asymmetric dynamically. This stabilized dynamics among monomers may contribute to the increased efficiency of Ca^{2+} transport in TRPV5-T563.

Author Manuscript Author Manuscript Author Manuscript Author Manuscript

As described in the Material and Methods section, PCA (55) was utilized to determine the collective motion of residues in TRPV5. To clearly show the change of collective motion between filter residues and residues (559-567) around residue 563 caused by the A563T variation, only the first eigenvectors that dominate the principal component of motion for the two group residues are shown in Figure 7. In TRPV5-A563 (Figure 7a), while no significant motion was observed for the residues in monomers 1 and 3, the residues around A563 exhibited departure motion between the opposite monomers 2 and 4 (black arrows in Figure 7a). This likely enlarges the TRPV5 pore. In contrast, the residues around T563 in monomers 2 and 4 of TRPV5-T563 exhibited motion toward each other. This may induce a tighter channel pore. Accompanied with the motions around A563, the filter residues in monomers 1 and 2 of TRPV5-A563 also showed departure motion away from those in monomers 3 and 4. In contrast, the filter residues in the four monomers of TRPV5-T563 showed collective motion in the same direction (red arrows in Figure 7b). This indicated that when Ca^{2+} ions were present in the pore, the A563T variation would result in closer filter residues. This is consistent with our fluctuation and coordinated motions results showing that the A563T variation may stabilize the TRPV5 pore. Possibly, this may lead to a higher efficiency for Ca^{2+} ions passing through the pore.

3.4 A563T variation alters the electrostatic potential in the outer surface of the TRPV5 pore

Electrostatic potential is an important factor in affecting the selectivity and transport of charged ions through channels (56). We calculated the electrostatic potential maps for TRPV5-A563 and -T563 (Figure 8). The negative potential is dominant on the outer surface of the TRPV5 pore, which attracts positively charged Ca^{2+} ions. When the alanine at 563 was substituted by threonine, the surface electrostatic negative potential of TRPV5-T563 became much smaller (Figure 8, left panels). In contrast to the change in the outer surface of the pore, the electrostatic potential in the inner pore was similar between TRPV5-A563 and TRPV5-T563 (Figure 8, right panels). The reduction of the outer electrostatic negative potential in the pore of TRPV5-T563 may reduce the energy required for Ca^{2+} ions to enter the inner pore and/or alter the interaction of the pore with Mg^{2+} ions. Although these data do not allow us to predict details of the interaction between the pore and cations, these changes are consistent with the alteration in Ca^{2+} uptake and Mg^{2+} sensitivity in the A563T variant of TRPV5.

3.5 A563T variation reduces the fluctuation of Ca^{2+} ions in the selective filter of the TRPV5 pore

In the initial simulation, the five Ca^{2+} ions (Ca1 to Ca5) modeled in TRPV5 were restrained in their original positions (Figure 1). During the production simulation, the restraints were removed to investigate whether the five Ca^{2+} ions remain in their initial sites. This was evaluated by calculating the time-dependent distance between each Ca^{2+} ion and the center of the selective filter (Figure S6a). In both systems, Ca1 and Ca2 moved away from their initial sites. In contrast, Ca3, Ca4 and Ca5 remained in the selective filter during the simulation. Compared to TRPV5-A563, the remaining three Ca^{2+} ions in TRPV5-T563 were closer to the center of the ion translocation path (Figure 4). The RMSF values, which reflect the dynamical change of Ca^{2+} ions in the selective filter, were lower in TRPV5-T563 than

Author Manuscript Author Manuscript Author Manuscript Author Manuscript

those in TRPV5-A563 (Figure S6b). This suggests that Ca^{2+} ions may have less horizontal movement along the ion translocation path of TRPV5-T563.

Both dynamical and structural asymmetry among the monomers of TRPV5 has been observed in this study, and this also helped to observe the differences between the TRPV5 variants (Figures 6, 7 and 8). The dynamical asymmetry is evident for the collective motions (PCA analysis in Figure 7). While one pair of diagonal opposite TM6 in TRPV5-T563 moved towards each other, that in TRPV5-A563 moved away from each other. PCA is usually used to investigate the long time dynamics of proteins (55). In MD simulation, both local fluctuations of each residue and collective motions among residues occur simultaneously. Using multivariate statistical analysis, PCA can extract the global and large collective motions from the local and fast motions. The collective motion often represents the long dynamics of a protein that is related to conformational change and functional motion in the protein. Thus, asymmetry of monomers indicated by the long trend dynamics may reveal the physiological character of TRPV5. Furthermore, helix occupancy in the region around residue 563 of TRPV5 also exhibited asymmetry in the monomers. Monomers 3 and 4 of TRPV5-A563 lost their helix structure in this region, whereas the corresponding helix structure was maintained in the four monomers of TRPV5-T563 (Figure 3 and Figure S5). Asymmetry for the monomers is not specific for TRPV5 as it has been observed in some voltage-gated Na^+ (57-59) and Ca^{2+} channels (60).

Our previous work indicates that A563T variation in TRPV5 increases Ca^{2+} influx and reduces Na^+ transport by increasing the Mg^{2+} sensitivity of the channel (14). Previous studies by others indicated that D542 is the key residue in the pore that determines Ca^{2+} selectivity and Mg^{2+} sensitivity (17, 18). Because A/T563 is located in TM6, 20 amino-acid residues away from D542 in the pore, it was unclear how the residue at 563 affects Ca^{2+} transport and Mg^{2+} sensitivity. The availability of the TRPV1 structure made it possible to obtain further insight into this matter. Our results show that it is possible that A/T563 interacts with V540, just one residue away from D542 in a neighboring subunit.

Our simulation was based on the alignment shown in Figure S1a where D542 of TRPV5 is aligned with D646 of TRPV1. The alignment is the same in the original study which determined the TRPV1 structure (19), and is consistent with the pore structure of Ca^{2+} permeable channels (TRPV1 and Ca_vAb). The alternative alignment, where D542 of TRPV5 is aligned with M644 of TRPV1 (Figure S1b), was better suited with KcsA and has been used to model TRPV5 when the TRPV1 structure was not available. In this model (Figure S2b), the position of D542 corresponds to V540 in our current model (Figure S2a). The finding that A/T563 interacts with V540 in the original model (Figure 2) suggests that D542 in the alternative model may interact directly with A/T563. To test this proposition, 400 ns simulations were performed based on the alternative model using the same parameters and conditions to our original model. The contact numbers between residue 563 and filter residues in the alternative model (Figure S9) indicate that only P544 exhibited robust interaction with residue 563 in TRPV5-A563; however, both P544 and I541 interacted significantly with 563 in TRPV5-T563. D542 didn't exhibit robust interaction with residue 563 in either TRPV5-A563 or TRPV5-T563 as we originally thought. Unlike V540, D542 was negatively charged and it was likely shifted toward the center of the pore where positive

Author Manuscript Author Manuscript Author Manuscript Author Manuscript

charged Ca^{2+} ions were present (Figure S9). This may explain why robust interaction between residue 563 and D542 didn't take place in the alternative model.

In addition, we also performed other structural (Figure S13), dynamical (Figures S10 and S12) and electrostatic (Figure S11) analyses for TRPV5-A563 and TRPV5-T563 using the alternative model, and results are summarized in the Supporting Information. Similar to the results observed in the original model, TRPV5-T563 exhibited lower surface electrostatic negative potential (Figure S11) and less collective motion of monomers (Figure S10) than TRPV5-A563. However, dynamical motion of D542 (Figure S12) and helix occupancy around residue 563 (Figure S13) didn't differ substantially between the two TRPV5 variants in the alternative model.

Our original model exhibited smaller RMSD values (Figure S7) and more helix occupancy (Figure S8) than the alternative one in the modeled region of TRPV5, indicating our original model had smaller deviations from the initial structure. However, it is not easy to examine which model is correct without structural data. The cysteine-disulfide cross-linking approach is a useful tool to study the structure of TRPV5. However, cysteine mutations around the residue D542 resulted in non-functional channels, and therefore it was impossible to determine the accessibility of these residues (24). In addition, the A563C mutant was also non-functional (24). Although this indicates the importance of residue 563, it also made it challenging to study the interactions between this residue and its neighboring residues. A study that determines the structure of TRPV5 is necessary to solve these issues.

It is important to understand the mechanism by which A563T variation alters Ca^{2+} transport of TRPV5. The A563T variation provides an example of a mutation in a residue not directly involved in forming the pore of the channel influencing the pore dynamically. In addition to the ion transport mechanism, the A563T variation may contribute to the unique renal Ca^{2+} conservation mechanisms in African descendants. Compared to Caucasians, despite lower levels of serum 25-hydroxyvitamin D (but the same level of free 25-hydroxyvitamin D) (61), African Americans have a higher bone density (62), a lower fracture risk (63), and a lower prevalence of kidney stones (64). These observations indicate that African Americans have unique mechanisms to conserve Ca^{2+}. Consistent with this, African Americans show lower urinary excretion of Ca^{2+} than whites (65-67). TRPV5 is expressed in the distal convoluted tubule and connecting tubule in the kidney, and plays an important role in determining how much Ca^{2+} is excreted into the urine (15, 16). A L530R mutation in TRPV5 was recently found to be associated with recurrent kidney stones (68). The A563T variation of TRPV5, which is expected to increase Ca^{2+} reabsorption, could contribute to the lower urinary Ca^{2+} excretion, and in turn, the lower prevalence of kidney stones and the higher bone mineral density in African Americans. Although A563T variation has a moderate allele frequency (10-15%) in African Americans, it may be one of multiple factors contributing to their lower urinary Ca^{2+} excretion. A detailed mechanistic understanding of the impact of this variation in TRPV5 will be helpful in finding new strategies to increase bone mineral density by enhancing Ca^{2+} reabsorption and to prevent kidney stone disease.

The molecular dynamics simulation approach reveals that the A563T variation may increase the nearby occupancy helical structure, and decrease the pore size as measured by the

Author Manuscript Author Manuscript Author Manuscript Author Manuscript

distance between diagonally opposed D542 residues. In addition, the A563T variation also affects the coordination motion of the residues around the pore, and decreases the negative potential difference at the outer surface of the pore. These alterations in the A563T variant provide a structural basis for the observed functional changes observed earlier. Furthermore, it also provides an interesting example that a distant residue could lead to changes in the pore.

The all-atom MD simulation approach used in this study provides the detailed structural and dynamical changes induced by the A563T variation. This level of resolution cannot be achieved by other approaches at present. However, it also consumes tremendous computational resources if the entire transmembrane region of TRPV5 is simulated. Even though this may be achieved eventually, it is not feasible to model the TRPV5 structure in its entirety at present. We chose the most relevant region in TRPV5, hoping that this would be sufficient to provide insights into how the A563T variation could alter the key residues forming the pore of TRPV5. However, as we learned from the current study, alteration of a distant residue may result in changes in other regions of the protein. Although the results obtained in this study provide a feasible explanation of how A563T variation affects the channel pore, our results are limited by the sequence divergence between TRPV5 and the TRPV1, the deletion of residues 604-626 in the TRPV1 structure template, and the choice of alignment between TRPV5 and TRPV1. Thus, further experimental and theoretical research is needed to confirm our results and provide more details of the structure of TRPV5 as well as changes caused by the A563T variation.

Supplementary Material

Refer to Web version on PubMed Central for supplementary material.

ACKNOWLEDGEMENTS

We thank the Alabama Supercomputer Center and Supercomputer facility at the University of Alabama at Birmingham for providing computational resources.

FUNDING INFORMATION

This work was supported in part by the National Institute of Diabetes and Digestive and Kidney Diseases (R01DK072154).

REFERENCES

1. Suzuki Y, Landowski CP, Hediger MA. Mechanisms and regulation of epithelial Ca^{2+} absorption in health and disease, Annu. Rev. Physiol. 2008; 70:257–271.
2. van de Graaf SFJ, Boullart I, Hoenderop JGJ, Bindels RJM. Regulation of the epithelial Ca^{2+} channels TRPV5 and TRPV6 by 1α,25-dihydroxy vitamin D_3 and dietary Ca^{2+} J. Steroid. Biochem. Mol. Biol. 2004:89–90. 303–308.
3. Berridge MJ, Lipp P, Bootman MD. The versatility and universality of calcium signalling. Nat. Rev. Mol. Cell. Biol. 2000; 1:11–21. [PubMed: 11413485]
4. Hoenderop JGJ, Nilius B, Bindels RJM. Calcium absorption across epithelia. Physiol. Rev. 2005; 85:373–422. [PubMed: 15618484]
5. Schoeber JPH, Hoenderop JGJ, Bindels RJM. Concerted action of associated proteins in the regulation of TRPVS and TRPV6. Biochem. Soc. Trans. 2007; 35:115–119. [PubMed: 17233615]

Author Manuscript Author Manuscript Author Manuscript Author Manuscript

6. Hsu YJ, Hoenderop JGJ, Bindels RJM. TRP channels in kidney disease. BBA-Mol. Basis Dis. 2007; 1772:928–936.
7. Boros S, Bindels RJM, Hoenderop JGJ. Active Ca^{2+} reabsorption in the connecting tubule. Pflugers Arch. 2009; 458:99–109. [PubMed: 18989697]
8. Nijenhuis T, Hoenderop JGJ, Nilius B, Bindels RJM. (Patho)physiological implications of the novel epithelial Ca^{2+} channels TRPV5 and TRPV6. Pflugers Arch. 2003; 446:401–409. [PubMed: 12748856]
9. Nijenhuis T, Hoenderop JGJ, Bindels RJM. TRPV5 and TRPV6 in Ca^{2+} (re)absorption: regulating Ca^{2+} entry at the gate. Pflugers Arch. 2005; 451:181–192. [PubMed: 16044309]
10. Peng JB. TRPV5 and TRPV6 in Transcellular Ca^{2+} Transport: Regulation, Gene Duplication, and Polymorphisms in African Populations. Adv. Exp. Med. Biol. 2011; 704:239–275. [PubMed: 21290300]
11. Van Cromphaut SJ, Rummens K, Stockmans I, Van Herck E, Dijcks FA, Ederveen A, Carmeliet P, Verhaeghe J, Bouillon R, Carmeliet G. Intestinal calcium transporter genes are upregulated by estrogens and the reproductive cycle through vitamin D receptor-independent mechanisms. J. Bone Miner. Res. 2003; 18:1725–1736. [PubMed: 14584880]
12. Akey JM, Eberle MA, Rieder MJ, Carlson CS, Shriver MD, Nickerson DA, Kruglyak L. Population history and natural selection shape patterns of genetic variation in 132 genes. PLoS Biol. 2004; 2:1591–1599.
13. Stajich JE, Hahn MW. Disentangling the effects of demography and selection in human history. Mol. Biol. Evol. 2005; 22:63–73. [PubMed: 15356276]
14. Na T, Zhang W, Jiang Y, Liang Y, Ma HP, Warnock DG, Peng JB. The A563T cariation of the renal epithelial calcium channel TRPV5 among African Americans enhances calcium influx. Am. J. Physiol. Renal. Physiol. 2009; 296:1042–1051.
15. Mensenkamp AR, Hoenderop JGJ, Bindels RJ. TRPV5, the Gateway to Ca^{2+} Homeostasis. Handb Exp Pharmacol. 2007; 179:207–220.
16. Na T, Peng JB. TRPV5: A Ca^{2+} Channel for the Fine-Tuning of Ca^{2+} Reabsorption. Handb Exp Pharmacol. 2014; 222:321–357. [PubMed: 24756712]
17. Nilius B, Vennekens R, Prenen J, Hoenderop JGJ, Droogmans G, Bindels RJM. The single pore residue Asp^{542} determines Ca^{2+} permeation and Mg^{2+} block of the epithelial Ca^{2+} channel. J. Biol. Chem. 2001; 276:1020–1025. [PubMed: 11035011]
18. Dodier Y, Dionne F, Raybaud A, Sauve R, Parent L.y. Topology of the selectivity filter of a TRPV channel: rapid accessibility of contiguous residues from the external medium. Am. J. Physiol., Cell Physiol. 2007; 293:C1962–C1970. [PubMed: 17942632]
19. Liao M, Cao E, Julius D, Cheng Y. Structure of the TRPV1 ion channel determined by electro cyo-microscopy. Nature. 2013; 504:107–112. [PubMed: 24305160]
20. Cao E, Liao M, Cheng Y, Julius D. TRPV1 structures in distinct conformations reveal activation mechanisms. Nature. 2013; 504:113–118. [PubMed: 24305161]
21. Sali A, Blundell TL. Comparative Protein Modeling by Satisfaction of Spatial Restraints. J. Mol. Biol. 1993; 234:779–815. [PubMed: 8254673]
22. Larkin MA, Blackshields G, Brown NP, Chenna R, McGettigan PA, McWilliam H, Valentin F, Wallace IM, Wilm A, Lopez R, Thompson JD, Gibson TJ, Higgins DG. ClustalW and ClustalX version 2. Bioinformatics. 2007; 23:2947–2948. [PubMed: 17846036]
23. Forrest LR, Tang CL, Honig B. On the accuracy of homology modeling and sequence alignment methods applied to membrane proteins. Biophys. J. 2006; 91:508–517. [PubMed: 16648166]
24. Dodier Y, Banderali U, Klein H, Topalak O, Dafi O, Simoes M, Bernatchez G, Sauve R, Parent L. Outer pore topology of the ECaC-TRPV5 channel by cysteine scan mutagenesis. J. Biol. Chem. 2004; 279:6853–6862. [PubMed: 14630907]
25. Yeh B, Kim YK, Jabbar W, Huang C. Conformational changes of pore helix coupled to gating of TRPV5 by protons. EMBO J. 2005; 24:3224–3234. [PubMed: 16121193]
26. Tang L, Gamal El-Din TM, Payandeh J, Martinez GQ, Heard TM, Scheuer T, Zheng N, Catterall WA. Structural basis for Ca^{2+} selectivity of a voltage-gated calcium channel. Nature. 2014; 505:56–61. [PubMed: 24270805]

Author Manuscript Author Manuscript Author Manuscript Author Manuscript

27. Colovos C, Yeates TO. Verification of protein structures: patterns of nonbonded atomic interactions. Protein Sci. 1993; 2:21511–21519.
28. Laskowski RA, Macarthur MW, Moss DS, Thornton JM. PROCHECK: a program to check the stereochemical quality of protein structures. J. Appl. Cryst. 1993; 26:283–291.
29. Hooft RWW, Vriend G, Sander C, Abola EE. Errors in protein structures. Nature. 1996; 381:272–272. [PubMed: 8692262]
30. Eisenberg D, Luthy R, Bowie JU. VERIFY3D: Assessment of protein models with three-dimensional profiles. Methods Enzymol. 1997; 277:396–404. [PubMed: 9379925]
31. Humphrey W, Dalke A, Schulten K. VMD: Visual molecular dynamics. J. Mol. Graphics Modell. 1996; 14:33–38.
32. The PyMOL. Molecular Graphics System. Version 1.5.0.4. Schrödinger, LLC;
33. Jo S, Lim JB, Klauda JB, Im W. CHARMM-GUI Membrane Builder for Mixed Bilayers and Its Application to Yeast Membranes. Biophys. J. 2009; 97:50–58. [PubMed: 19580743]
34. Hornak V, Abel R, Okur A, Strockbine B, Roitberg A, Simmerling C. Comparison of multiple amber force fields and development of improved protein backbone parameters. Proteins. 2006; 65:712–725. [PubMed: 16981200]
35. Dickson CJ, Madej BD, Skjevik AA, Betz RM, Teigen K, Gould IR, Walker RC. Lipid14: The Amber Lipid Force Field. J. Chem. Theory Comput. 2014; 10:865–879. [PubMed: 24803855]
36. Case, DA., Babin, V., Berryman, JT., Betz, RM., Cai, Q., Cerutti, DS., Cheatham, I., T.E., Darden, TA., Duke, RE., Gohlke, H., Goetz, AW., Gusarov, S., Homeyer, N., Janowski, P., Kaus, J., Kolossváry, I., Kovalenko, A., Lee, TS., LeGrand, S., Luchko, T., Luo, R., Madej, B., Merz, KM., Paesani, F., Roe, DR., Roitberg, A., Sagui, C., Salomon-Ferrer, R., Seabra, G., Simmerling, CL., Smith, W., Swails, J., Walker, RC., Wang, J., Wolf, RM., X., W., Kollman, PA. AMBER 14. University of California; San Francisco: 2014.
37. Berendsen HJC, Postma JPM, van Gunsteren WF, DiNola A, Haak JR. Molecular dynamics with coupling to an external bath. J. Chem. Phys. 1984; 81:3684–3690.
38. Ryckaert J-P, Ciccotti G, Berendsen HJC. Numerical integration of the cartesian equations of motion of a system with constraints: Molecular dynamics of n-alkanes. J. Comput. Phys. 1977; 23:327–341.
39. Darden T, York D, Pedersen L. Particle Mesh Ewald - an N.Log(N) Method for Ewald Sums in Large Systems. J Chem Phys. 1993; 98:10089–10092.
40. Essmann U, Perera L, Berkowitz ML, Darden T, Lee H, Pedersen L. A smooth particle mess Ewald method. J. Chem. Phys. 1995; 103:8577–8593.
41. Kabsch W, Sander C. Dictionary of protein secondary structure: pattern recognition of hydrogen-bonded and geometrical features. Biopolymers. 1983; 22:2577–2637. [PubMed: 6667333]
42. Feig, M., Karanicolas, J., Brooks, I., C. L.. MMTSB NIH Research Resource. The Scripps Research Institute; 2001. MMTSB Tool set.
43. MacQueen, JB. Some Methods for classification and Analysis of Multivariate Observations. Proceedings of 5-th Berkeley Symposium on Mathematical Statistics and Probability Berkeley; University of California Press; 1967. p. 281-297.
44. Arnold GE, Ornstein RL. Molecular dynamics study of time-correlated protein domain motions and molecular flexibility: Cytochrome P450BM-3. Biophys. J. 1997; 73:1147–1159. [PubMed: 9284282]
45. MATLAB. MathWorks. Natick, MA: 2013.
46. Lange OF, Grubmuller H. Full correlation analysis of conformational protein dynamics. Proteins. 2008; 70:1294–1312. [PubMed: 17876828]
47. Cheng Y, Lindert S, Kekenes-Huskey P, Rao VS, Solaro RJ, Rosevear PR, Amaro R, McCulloch AD, McCammon JA, Regnier M. Computational Studies of the Effect of the S23D/S24D Troponin I Mutation on Cardiac Troponin Structural Dynamics. Biophys. J. 2014; 107:1675–1685. [PubMed: 25296321]
48. Baker NA, Sept D, Joseph S, Holst MJ, McCammon JA. Electrostatics of nanosystems: Application to microtubules and the ribosome. Proc. Natl. Acad. Sci. USA. 2001; 98:10037–10041. [PubMed: 11517324]

Author Manuscript Author Manuscript Author Manuscript Author Manuscript

49. Allen, MP., Tildesley, DJ. Computer Simulation of Liquids. Oxford University Press; New York: 1987.
50. Lee SJ, Song Y, Baker NA. Molecular dynamics simulations of asymmetric NaCl and KCl solutions separated by phosphatidylcholine bilayers: potential drops and structural changes induced by strong Na^+-lipid interactions and finite size effects. Biophys. J. 2008; 94:3565–3576. [PubMed: 18222999]
51. Efron, B., Tibshirani, RJ. An Introduction to the Bootstrap. Chapman & Hall; New York: 1998.
52. Wang L, Murphy-Ullrich JE, Song Y. Molecular insight for the effect of lipid bilayer environments on thrombospondin-1 and calreticulin interactions. Biochemistry. 2014; 53:6309–6322. [PubMed: 25260145]
53. Bailey, NTJ. Statistical methods in biology. third edition ed. Cambridge University Press; New York, NY: 1995.
54. Voets T, Janssens A, Prenen J, Droogmans G, Nilius B. Mg^{2+}-dependent gating and strong inward rectification of the cation channel TRPV6. J. Gen. Physiol. 2003; 121:245–260. [PubMed: 12601087]
55. Balsera MA, Wriggers W, Oono Y, Schulten K. Principal component analysis and long time protein dynamics. J. Phys. Chem. 1996; 100:2567–2572.
56. Lin H, Tang H, Cai W. Accuracy and efficiency in computing electrostatic potential for an ion channel model in layered dielectric/electrolyte media. J. Comput. Phys. 2014; 259:488–512.
57. Payandeh J, Gamal El-Din TM, Scheuer T, Zheng N, Catterall WA. Crystal structure of a voltage-gated sodium channel in two potentially inactivated states. Nature. 2012; 486:135–139. [PubMed: 22678296]
58. Zhang X, Ren W, DeCaen P, Yan C, Tao X, Tang L, Wang J, Hasegawa K, Kumasaka T, He J, Clapham DE, Yan N. Crystal structure of an orthologue of the NaChBac voltage-gated sodium channel. Nature. 2013; 486:130–135.
59. Zhang X, Xia M, Li Y, Liu H, Jiang X, Ren W, Wu J, DeCaen P, Yu F, Huang S, He J, Clapham DE, Yan N, Gong H. Analysis of the selectivity filter of the voltage-gated sodium channel Na_vRh. Cell Res. 2013; 23:409–422. [PubMed: 23247626]
60. Koch SE, Bodi I, Schwartz A, Varadi G. Architecture of Ca^{2+} channel pore-linging segments revealed by covalent modification of substitued cysteines. J. Biol. Chem. 2000; 275:34493–34500. [PubMed: 10950957]
61. Aloia J, Mikhai M, Dhaliwal R, Shieh A, Usera G, Stolberg A, Raqolia L, Islam S. Free 25(OH)D and the Vitamin D paradox in African Americans. J. Clin. Endocrinol. Metab. 2015; 100:3356–3363. [PubMed: 26161453]
62. Harris SS, Wood MJ, Dawson-Hughes B. Bone mineral density of the total body and forearm in premenopausal black and white women. Bone. 1995; 16:311S–315S. [PubMed: 7626320]
63. Baron JA, Barrentt J, Malenka D, Fisher E, Kniffin W, Bubolz T, Tosteson T. Racial differences in fracture risk. Epidemiology. 1994; 5:42–47. [PubMed: 8117781]
64. Stamatelou KK, Francis ME, Jones CA, Nyberg LM, Curhan GC. Time trends in reported prevalence of kidney stones in the United States: 1976-1994. Kidney Int. 2003; 63:1817–1823. [PubMed: 12675858]
65. Pratt JH, Manatunga AK, Peacock M. A comparison of the urinary excretion of bone resorptive products in white and black children. J. Lab. Clin. Med. 1996; 127:67–70. [PubMed: 8592098]
66. Braun M, Palacios C, Wiqertz K, Jackman LA, Bryant RJ, McCabe LD, Martin BR, McCabe GP, Peacock M, Weaver CM. Racial differences in skeletal calcium retention in adolescent girls with varied controlled calcium intakes. Am. J. Clin. Nutr. 2007; 85:1657–1663. [PubMed: 17556706]
67. Taylor EN, Curhan GC. Differences in 24-hour urine composition between black and white women. J. Am. Soc. Nephrol. 2007; 18:654–659. [PubMed: 17215441]
68. Oddsson A, Sulem P, Helgason H, Edvardsson VO, Thorleifsson G, Sveinbjörnsson G, Haraldsdottir E, Eyjolfsson GI, Sigurdardottir O, Olafsson I, Masson G, Holm H, Gudbjartsson DF, Thorsteinsdottir U, Indridason OS, Palsson R, Stefansson K. Common and rare variants associated with kidney stones and biochemical traits. Nat. Commun. 2015; 6:7975–7983. [PubMed: 26272126]

Author Manuscript Author Manuscript Author Manuscript Author Manuscript

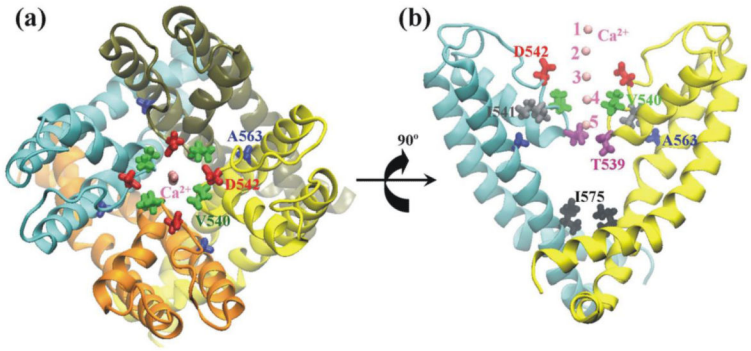

Figure 1. Initial modeled structure of the TRPV5 pore from a top view (a) or side view (b)

Only two diagonally opposed monomers are shown in Figure (b) for clarity. The structure was modeled based on the structure of TRPV1 using homology modeling. The TRPV5 sequence used in the modeling is shown in Figure S1a. Each monomer of TRPV5 is represented by a unique color (cyan, yellow, tan, and orange, respectively). Residues A563 (blue), filter residues (T539 (purple), V540 (green), I541 (grey), and D542 (red)), residue I575 (black) and five Ca^{2+} ions (pink) in TRPV5 are indicated.

Author Manuscript Author Manuscript Author Manuscript Author Manuscript

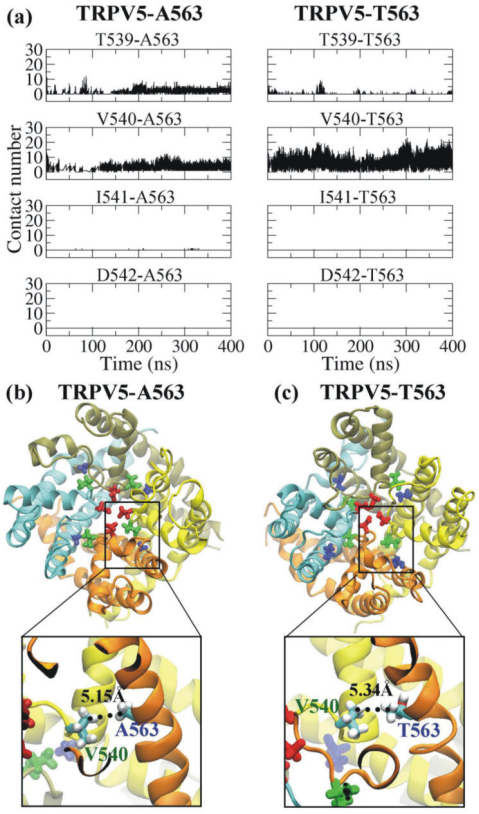

Figure 2. Interaction between V540 and residue 563 in the neighboring subunit

(a)Time-dependent contact number between each filter residue and residue 563 in TRPV5-A563 (left) and TRPV5-T563 (right). (b) and (c), Representative structures exhibiting the interaction between V540 and A/T563. The residue colors are the same to those in Figure 1. To clearly show the interaction, the view of the enlarged figure is oriented, and the carbon and hydrogen atoms for V540 and A/T563 in the center of the enlarged figures are colored in cyan and white, respectively. Distance between a V540 and its neighboring residue 563 is shown in the enlarged figures.

Author Manuscript Author Manuscript Author Manuscript Author Manuscript

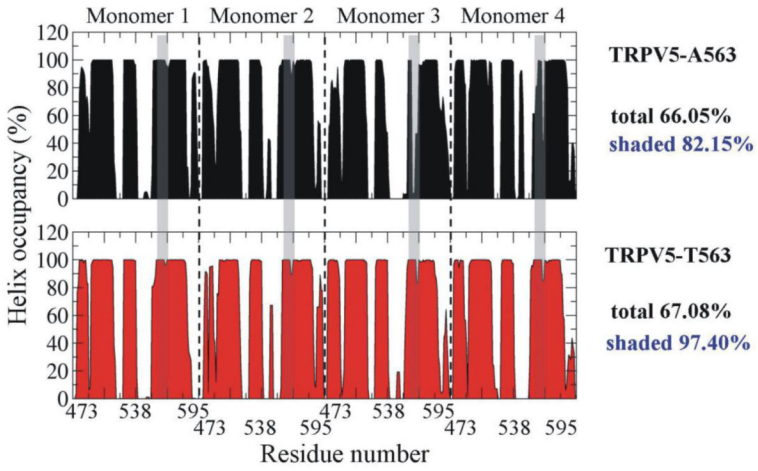

Figure 3. Residues of α-helix occupancy of TRPV5-A563 and TRPV5-T563

The overall percentage helix of the region covering amino-acid residues 473-595 in each of the four monomers of TRPV5 was calculated and expressed as the overall helicity in that region divided by the total residue number of that region. The shaded region represents residues 559 to 567 around A563 (upper panel) or T563 (lower panel) in each TRPV5 monomer.

Author Manuscript Author Manuscript Author Manuscript Author Manuscript

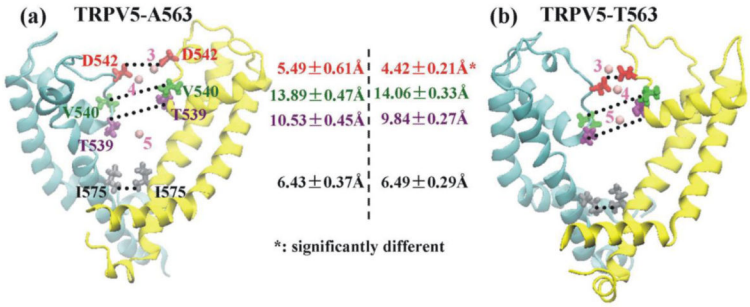

Figure 4. Distances between key residues in the diagonally opposed subunits of TRPV5-A563 (a) and TRPV5-T563 (b)

The distance is averaged from the two different diagonally opposed subunit groups. Distances between diagonally opposed carboxylate oxygen atoms of D542, between diagonally opposed backbone carbon atoms of V540, between diagonally opposed carbonyl oxygen atoms of T539, and between diagonally opposed side chain carbon atoms of I575 are shown.The standard deviation was calculated based on the statistically independent periods of MD simulation trajectories as described in Statistical methods in the Materials and Method section. * indicates that the difference is statistically significant based on the mean and standard deviation of the analyzed variable (Student's t-test, $p < 0.05$). Three Ca^{2+} ions remained inside the channel (Ca3, Ca4 and Ca5) are shown in the figures.

Author Manuscript Author Manuscript Author Manuscript Author Manuscript

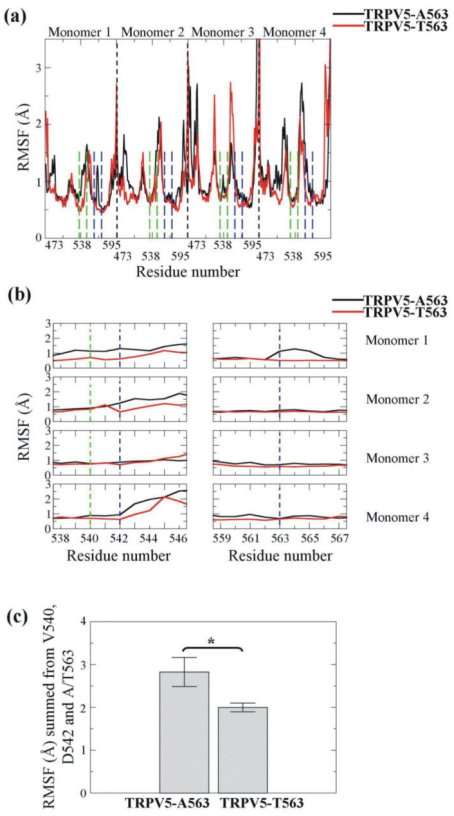

Figure 5. Root mean square fluctuation (RMSF) comparisons between TRPV5 variants

(a) RMSF comparison for the four monomers of TRPV5. Monomers are separated by black dashed lines. The regions between green dashed lines and between blue dashed lines are zoomed in and shown in the left and right panels of Figure b, respectively. (b) RMSF comparison for residues around D542 (left panel) and around residue 563 (right panel). The green and blue dashed lines in the left panel indicate the positions of V540 and D542, respectively. The blue dashed line in the right panel indicates the position of A/T563. (c) The RMSF values summed from V540, D542 and residue 563 of TRPV5-T563 are significantly lower than those of TRPV5-A563. The standard deviation was calculated based on the statistically independent periods of MD simulation trajectories as described in Statistical methods in the Materials and Method section. * indicates that the difference is statistically significant based on the mean and standard deviation of the analyzed variable (Student's t-test, $p < 0.05$).

Author Manuscript Author Manuscript Author Manuscript Author Manuscript

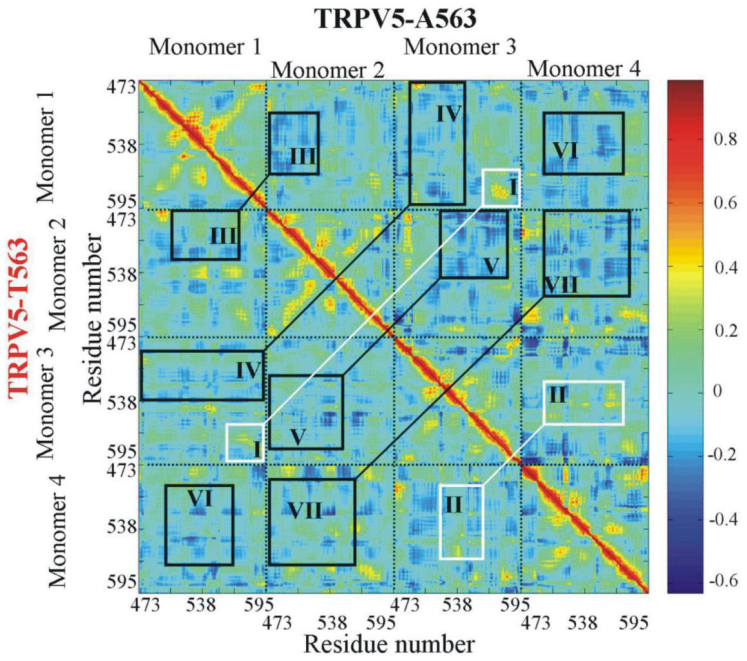

Figure 6. Dynamical cross-correlation maps (DCCM) for the comparison of the degree of correlated motion of the residues in TRPV5-A563 (top right) and TRPV5-T563 (bottom left)

The red color shows the correlation between residues, whereas the blue color shows the anticorrelation between residues. The changed regions of positive correlation are represented in white boxes, whereas the changed regions of anticorrelation in black boxes.

Author Manuscript Author Manuscript Author Manuscript Author Manuscript

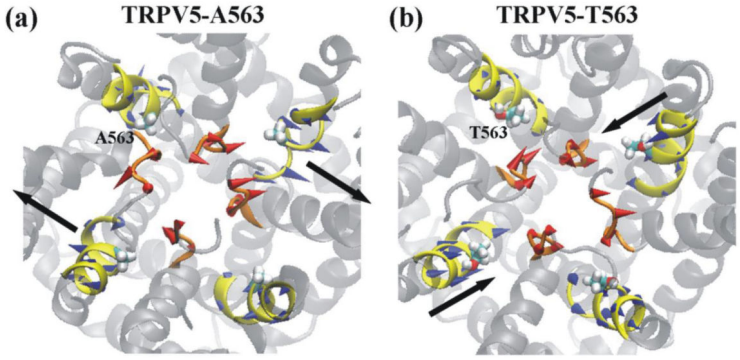

Figure 7. Principal component analysis (PCA) for the comparison of the collective motion between TRPV5-A563 (a) and TRPV5-T563 (b)

Red arrows indicate the motion of filter residues (in orange) along the first PC, while blue arrows indicate the motion of residues around A/T563 (in yellow) along the first PC. Black arrows represent the difference of collective motion between TRPV5-A563 and TRPV5-T563.

Author Manuscript Author Manuscript Author Manuscript Author Manuscript

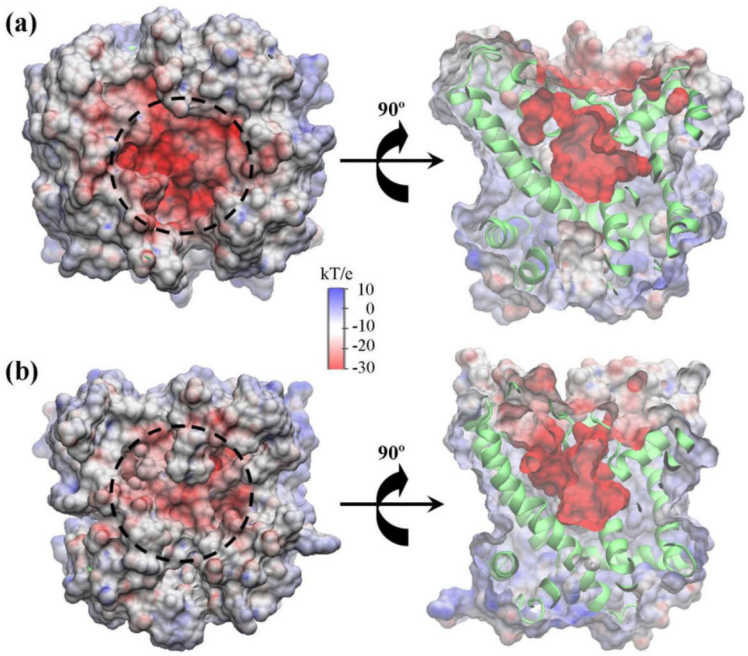

Figure 8. Comparison of the electrostatic potential between TRPV5-A563 (a) and TRPV5-T563 (b)

Top view of the surface electrostatic potential for TRPV5 pore is shown in the left figure, whereas side view of the electrostatic potential projected on the inner pore's van der Waals surface is shown in the right figure. Dashed circles indicate the outer surface of channel pore.